EDGE EFFECTS IN THIN FILM DELAMINATION

H. H. YU[1], M. Y. HE[2] and J. W. HUTCHINSON[1]*

[1]Division of Engineering and Applied Sciences, Harvard University, Cambridge, MA 02138, USA and
[2]Material Engineering Department, University of California, Santa Barbara, CA 93106, USA

Abstract—Thin films bonded to a substrate often sustain large in-plane residual stresses that are transferred to the film via shear stresses on the interface near their edges. These edge zones play a significant role in film delamination. A new method is introduced to analyze both the residual stress distribution in a film near its edge and the energy release rate and mode mix for an interface delamination crack emerging from, or converging upon, an edge. Two two-dimensional configurations are considered: (a) a film whose edge lies in the interior of the substrate and (b) a film whose edge is aligned with the edge of the substrate (i.e. the film/substrate geometry is a quarter-plane). There are significant differences between the two cases. For the former, (a), the energy release rate approaches the steady-state, limiting rate for a long interface crack when the crack has extended less than one film thickness. By contrast, the energy release rate in case (b) remains far below the steady-state rate until the crack extends to ten or more film thicknesses from the edge. In case (b), the edge effect provides a significant protection against edge delamination, whereas in case (a) it does not. Elastic mismatch between the film and the substrate is significant in case (b), but not in case (a). A second set of behaviors is investigated wherein the interface crack approaches the edge of the film from the interior. For both types of edges, the energy release rate drops well below the steady-state rate at remaining ligament lengths that are very large compared to the film thickness, approaching zero as the delamination converges on the edge. Analytic features which account for the various behaviors will be highlighted, and practical implications for thin film delamination will be discussed. © 2001 Acta Materialia Inc. Published by Elsevier Science Ltd. All rights reserved.

Keywords: Thin films; Delamination

1. INTRODUCTION

Thin films are often employed in a stressed state. The origins of the stress can be epitaxy, growth processes (e.g. crystalline coalescence in physical or chemical vapor deposition), thermal expansion mismatch, differential densification (e.g. constrained sintering), and others. In some applications the magnitude of the stress can be as large as several GPa. The stress is transferred to the film via shear stress on the interface near the film edges (Fig. 1). The stress concentration near the edge makes the film susceptible to delamination from the substrate. When the stress in the film is compressive, buckling above an initial interface flaw may provide enough driving force to delaminate the film. When the film is in residual tension, delamination can initiate preferentially along the film edge [1]. The present work assumes that the film is under uniform tension with magnitude σ_0 well away from the edge, directed perpendicularly to the crack edge.
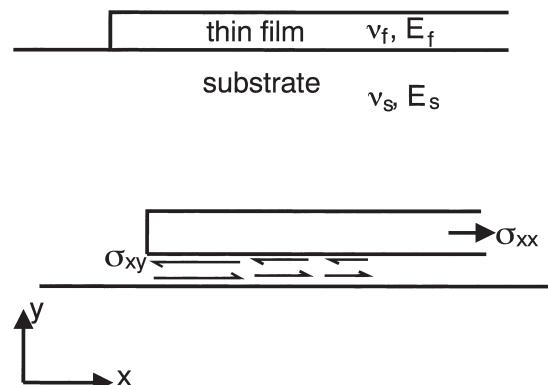
Fig. 1. Film/substrate system illustrating the role of the shear traction on the interface near the edge of the film.

The component of stress parallel to the crack edge does not influence any of the results presented in the paper. Thus, for example, the results will apply to a film under an equi-biaxial stress state σ_0 or to a film that is only stressed perpendicularly to the edge.

When the tip of an interface edge crack (Fig. 2) is sufficiently far away from the edge, steady-state
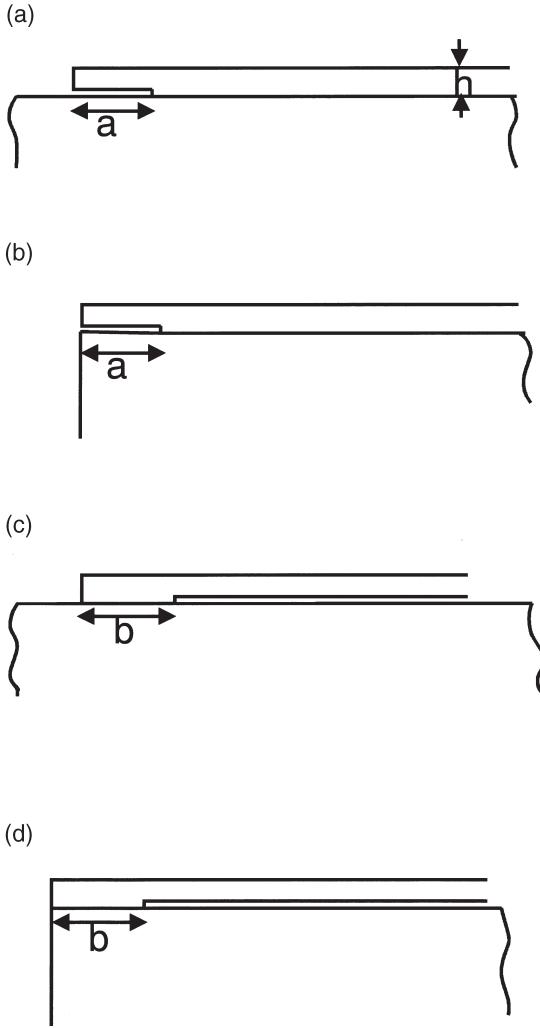
Fig. 2. Four geometries studied in this paper. Delaminations emerging from the film edge: (a) interior edge, and (b) edge at a corner. Delaminations converging on an edge: (a) interior edge, and (b) edge at a corner.

propagation prevails with energy release rate independent on crack length being

$$G_{ss} = \frac{(1-v_f^2)\sigma_0^2 h}{2E_f}, \qquad (1)$$

with E_f and v_f as the Young's modulus and Poisson's ratio of the film, and h the film thickness. This is simply the elastic energy per unit area in the film released, subject to the plane strain constraint. If $G_{ss} > \Gamma_i$, where Γ_i is the interface toughness at the relevant mode mix, spontaneous thin film delamination would be expected to occur given a sufficiently large initial crack. Whether or not this happens will depend on the initiation conditions along the edges, which is one of the main motivations underlying the present study.

Two two-dimensional plane strain configurations are considered in this paper: (a) a semi-infinite film whose edge lies in the interior of the substrate plane (Fig. 2(a)), and (b) a semi-infinite film whose edge is aligned with the edge of the substrate (i.e. the film/substrate geometry is a quarter-plane) (Fig. 2(b)). Previous studies have discussed some aspects of these problems, but have not uncovered the significant differences between them [1, 2]. If the film/substrate system has $G_{ss} > \Gamma_i$, the edge effect in case (b) provides a substantial barrier to the initiation of edge delaminations, but not in case (a).

The film displays a different type of behavior when the crack approaches one film edge from interior (Fig. 2(c) and (d)). The crack tip and the edge "sense" each other from a remarkably large distance. As they become close, the remaining residual stress in the film decreases and the energy release rate drops. A propagating interface crack ($G_{ss} > \Gamma_i$) will stop as it approaches an edge when the energy release rate drops to the level of the interface toughness. Zhuk *et al.* [3] exploited this edge effect in the experimental measurement of the interface toughness of a Ni-polymer bi-layer bonded to a silicon substrate. He, Evans and Hutchinson [4] termed such behavior "convergent debonding" and showed that it also arises in contexts other than thin films. The method developed in this paper is used to study the two cases in Fig. 2(c) and (d).

The residual stress distribution itself can affect the non-mechanical properties of microelectronic devices (e.g. Ramirez *et al.* [5]). For this reason we devote some attention to the determination of the residual stress distribution in the film in the vicinity of an edge, although not at the finest level. When two film edges (or a crack and an edge) are close, each edge senses the other and the residual stress in the film drops. The interaction will be displayed, providing further insight into the behavior underlying convergent debonding.

Another motivation underlying the present paper is the desire to develop a simple and reliable method for analyzing thin films. A thin film on a substrate is similar in some respects to the problem of a stiffener on a sheet or half plane [6, 7]. The membrane model used for stiffeners has been used to describe thin films [8]. In the membrane model, only shear traction on the interface is considered while normal traction is ignored. While it captures certain features of the behavior with fidelity, this model does not give the right mode mix when a crack emerges from the edge. Moreover, the shear stress distribution prediction along the interface is less accurate than might be desired. Shield and Kim [9] used elementary beam theory (or, equivalently, plate theory) to model the film, thereby introducing the normal traction on the interface. This model gives rise to a complex stress singularity at the crack tip, even when the thin film and the substrate are the same material. The model that will be introduced in this paper is constructed to give the exact form of the singularity at the interface

crack tip. It employs beam (or plate) theory in one step of the analysis, but it does so in a way that does not introduce significant quantitative errors. While the new model is slightly more complicated to describe than the earlier models, its formulation and the numerical method required for its solution are each quite similar.

The plan of this paper is as follows: In Section 2, the new thin film model is introduced and the governing equations for problems in Fig. 2 are formulated. Section 3 provides the results that distinguish between the edge conditions in the two cases. Stress distributions for finite width films are reported in Section 4, highlighting the interaction between the edges. Convergent debonds are studied in Section 5. The paper concludes with other illustrations in Section 6.

2. THE MODEL

The reference residual stress in the film remote from the ends is assumed to be uniform and tensile when the width of the film is sufficiently great. This reference residual stress, σ_0, is assumed to be due to a strain mismatch between the film and substrate. For a thin film with finite width, $2L$, a standard representation introduced for analysis purposes employs the superposition of a uniformly stressed film (Fig. 3(a)) with the "reduced problem" (Fig. 3(b)) wherein the film is attached to the substrate and subject to a compressive loading σ_0 on its ends. Since the problem of Fig. 3(a) is trivial, attention shifts to the solution of the reduced problem. Denote the traction components along the interface between the film and substrate by

$\sigma_{yy}(x)$ and $\sigma_{xy}(x)$. The plane strain version of the reduced problem in Fig. 3(b) is under consideration here.

The essential step in the new model is the representation of the reduced problem as the sum of the three sub-problems shown in Fig. 4: the trivial problem for the free-standing film under uniform compression in Fig.4(a); a semi-infinite upper half space with the properties of the film and subject to tractions $\sigma_{yy}(x)$ and $\sigma_{xy}(x)$ in the interval $(-L, L)$ along its bottom in Fig. 4(b); and a free-standing film with specially chosen tractions along the three faces indicated in Fig. 4(c). The tractions on the three surfaces in Fig. 4(c) are chosen to be equal and opposite those induced in the problem of Fig. 4(b) along the same three planes defining the film. With this choice, it is clear that the superposition of the three problems gives precisely the desired traction conditions indicated for the reduced problem at the top of Fig. 4. The problems in Fig. 4(a) and (b) will be solved exactly, and the substrate is treated exactly in coupling it to the combination of sub-problems in Fig. 4. If the problem in Fig. 4(c) were solved exactly, the superposition of the three solutions would provide the exact solution to the reduced problem. Instead, we will solve the problem in Fig. 4(c) approximately using beam (plate) theory to represent the film. We will demonstrate that this approximation introduces relatively little inaccuracy in the quantities of interest in this paper.

Fig. 3. Definition of the reduced problem in (b).
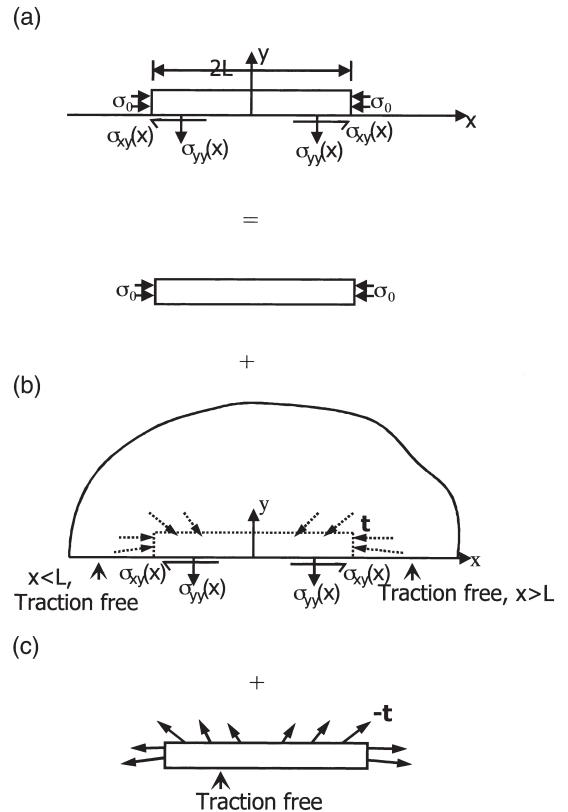
Fig. 4. Three sub-problems used in constructing the solution to the reduced problem.

The solutions of Fig. 4(a) and (b) are well known. Let (u, v) be the displacement components on the interface. In Fig. 4(a),

$$(du/dx)^{(a)} = -\frac{\sigma^o}{\bar{E}_f}, \quad (dv/dx)^{(a)} = 0, \qquad (2)$$

where $\bar{E} = E/(1 - v^2)$. The superscript (a) denotes the contribution from the problem in Fig. 4(a) in the superposition procedure. The superscripts (b) and (c) are used next for contributions from the problems in Fig. 4(b) and (c).

For the half plane problem depicted in Fig. 4(b), the expressions for the derivatives of displacement along the interface are known in terms of $\sigma_{yy}(x)$ and $\sigma_{xy}(x)$:

$$(du/dx)^{(b)} = \frac{1 - 2v_f}{1 - v_f}\frac{\sigma_{yy}(x)}{\bar{E}_f} - \frac{2}{\pi\bar{E}_f}\int_{-L}^{L}\frac{\sigma_{xy}(\xi)}{\xi - x}d\xi \quad (3a)$$

$$(dv/dx)^{(b)} = -\frac{1 - 2v_f}{1 - v_f}\frac{\sigma_{xy}(x)}{\bar{E}_f} - \frac{2}{\pi\bar{E}_f}\int_{-L}^{L}\frac{\sigma_{yy}(\xi)}{\xi - x}d\xi, \qquad (3b)$$

where the integrals exist in the sense of their Cauchy principal values. Traction free condition along the surface outside the interval $(-L, L)$ has been accounted for in equation (3).

The problem in Fig. 4(c) is solved using beam (wide plate) theory. Again, the objective is to obtain a representation analogous to equation (2) and equation (3) for the expressions of the derivatives of the displacements. The applied tractions in Fig. 4(c) are those needed to cancel the tractions on the corresponding surface cuts (dashed lines) in Fig. 4(b), as illustrated in Fig. 5. Consider a normal traction $\sigma_{yy}(\xi)$ exerted on a line element $d\xi$ along the bottom at position $(\xi, 0)$ in Fig. 5(a). From the point force solution (see [10]), the induced tractions on the other three surfaces all "radiate" from the point $(\xi, 0)$ (Fig. 5(a)). Consider a cross section in Fig. 5(b) at position x. The resultant forces per unit thickness equivalent to the reversed tractions (Fig. 5(b)) to the left of the cross section, dF_x and dF_y, are

$$dF_x = \frac{\sigma_{yy}(\xi)d\xi}{2\pi}(1 - \cos 2\alpha) \qquad (4a)$$

$$dF_y = -\frac{\sigma_{yy}(\xi)d\xi}{2\pi}(2\pi - 2\alpha + \sin 2\alpha) \qquad (4b)$$

where $\alpha = \cotan^{-1}[(x - \xi)/h]$ lies between 0 and π.

(a)

(b)
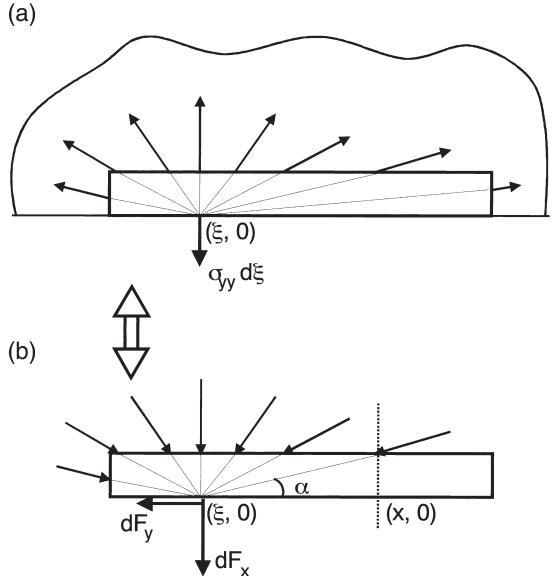
Fig. 5. Details of the conventions for sub-problems (b) and (c) in Fig. 4.

The resultant forces are exerted at point $(\xi, 0)$ (Fig. 5(b)). The corresponding moment at the cross section caused by the resultant forces is

$$dM = dF_x{\cdot}h/2 - dF_y{\cdot}(x - \xi) \qquad (5)$$

The resultant forces and moment corresponding to the shear traction on the interface in Fig. 5(b) can be obtained by the same procedure. The transverse stress σ_{xx} at point x on the interface in Fig. 5(b) is estimated by integrating along the interface with respect to ξ to include the contributions from all the tractions along the interface in Fig. 4(b):

$$\sigma_{xx}(x) = -\int_{-L}^{L}\left(\frac{dF_x}{h} + \frac{hdM}{2\bar{E}_f I}\right), \qquad (6)$$

where $I = h^3/12$ is the bending inertia for a unit thickness of depth. The first term in the integral corresponds to the average stress at the cross section, and the second is the stress caused by bending moment.

Adding the contributions from both the shear and normal tractions, one obtains the derivatives of the displacements along the interface in Fig. 5(b):

$$(du/dx)^{(c)} = \frac{1}{2\pi\bar{E}_f}\int_{-L}^{L}\left[4\frac{-\sin 2\alpha + 2\pi - 2\alpha}{h}\right.$$
$$\left. + 6\frac{(1 - \cos 2\alpha)(x - \xi)}{h^2}\right]\sigma_{xy}(\xi)d\xi \qquad (7a)$$
$$+ \frac{1}{2\pi\bar{E}_f}\int_{-L}^{L}\left[4\frac{\cos 2\alpha - 1}{h}\right.$$

$$-6\frac{(\sin 2\alpha + 2\pi - 2\alpha)(x-\xi)}{h^2}\bigg]\sigma_{yy}(\xi)d\xi$$

and

$$(dv/dx)^{(c)} = -\int_{-L}^{x}\frac{M}{\bar{E}_f I}dx + \theta_0, \qquad (7b)$$

with

$$M(x) = -\int_{-L}^{L}[(1-\cos 2\alpha)(x-\xi) + (-\sin 2\alpha$$

$$+ 2\pi - 2\alpha)h/2]\frac{\sigma_{xy}(\xi)}{2\pi}d\xi + \int_{-L}^{L}[(\sin 2\alpha + 2\pi \quad (8)$$

$$-2\alpha)(x-\xi) + (1-\cos 2\alpha)h/2]\frac{\sigma_{yy}(\xi)}{2\pi}d\xi.$$

In equation (7b), θ_0 is a constant to be determined. The three contributions to the derivatives of displacements in the film along the interface, equations (2), (3) and (7) combine to give

$$(du/dx)^{(f)} = (du/dx)^{(a)} + (du/dx)^{(b)} + (du/dx)^{(c)} \qquad (9a)$$

$$(dv/dx)^{(f)} = (dv/dx)^{(a)} + (dv/dx)^{(b)} + (dv/dx)^{(c)}, \qquad (9b)$$

where the superscription (f) stands for film.

For configurations in Fig. 2(a) and (c), the substrate is a semi-infinite half plane and the derivatives of the displacement along the interface are,

$$(du/dx)^{(s)} = \frac{1-2v_s}{1-v_s}\frac{\sigma_{yy}(x)}{\bar{E}_s} + \frac{2}{\pi\bar{E}_s}\int_{-L}^{L}\frac{\sigma_{xy}(\xi)}{\xi-x}d\xi \qquad (10a)$$

$$(dv/dx)^{(s)} = -\frac{1-2v_s}{1-v_s}\frac{\sigma_{xy}(x)}{\bar{E}_s} + \frac{2}{\pi\bar{E}_s}\int_{-L}^{L}\frac{\sigma_{yy}(\xi)}{\xi-x}d\xi, \qquad (10b)$$

where superscript (s) stands for "substrate". Again the integral is in the interval $(-L, L)$ due to the traction free condition outside the interval.

The displacements and the tractions are continuous along the bonded interface, the integral equations governing the interface tractions are obtained from the conditions $(du/dx)^{(f)} = (du/dx)^{(s)}$ and $(dv/dx)^{(f)} = (dv/dx)^{(s)}$. The tractions along the interface should also satisfy three overall equilibrium conditions for zero net force and zero net moment acting on the interface:

$$\int_{-L}^{L}\sigma_{xy}(\xi)d\xi = 0 \qquad (11a)$$

$$\int_{-L}^{L}\sigma_{yy}(\xi)(\xi + L)d\xi = 0 \qquad (11b)$$

$$\int_{-L}^{L}\sigma_{yy}(\xi)d\xi = 0. \qquad (11c)$$

The Cauchy-type integral equations for the tractions are solved numerically using the method introduced in [11]. The displacement jump behind the crack tip can be obtained using equation (9) and equation (10), once the tractions have been obtained.

The decomposition of the reduced problem depicted in Fig. 4 applies as well to the cases involving interface cracks. In these cases, the use of the semi-infinite half space in the sub-problem in Fig. 4(b) ensures that the form of the interface singularity is exactly that of the original problem. This is one of the essential steps which helps ensure the accuracy of the method. The other is that none of the loads in the problem of Fig. 4(c) act on the bottom of the film or near the crack tip. This is important in ensuring the accuracy of the beam approximation used in obtaining equation (7). Finally, while we have introduced an extra problem in the form of the half-space in Fig. 4(b), its solution is well known and the coupling to the lower half space representing the substrate leads to integral equations which are similar in form to those emerging in the earlier methods.

For a semi-infinite thin film, a superposition procedure similar to that in Fig. 4 and Fig. 5 is readily constructed. Now, the net surface tractions will be balanced by the stress in the film at infinity. The final expressions for the tangential derivatives of the displacements along the interface remain the same, except the lower and upper limit of the integrals are now 0 and ∞ with $x = 0$ as the left end of the film. The conditions expressed by equation (11a) and equation (11b) are replaced by

$$\int_{0}^{\infty}\sigma_{xy}(\xi)d\xi = \sigma_0 h \qquad (12a)$$

$$\int_0^\infty \sigma_{yy}(\xi)\xi d\xi = -\sigma_0 h^2/2. \qquad (12b)$$

If the substrate is a quarter plane (Fig. 2(b) and (d)), the derivatives of the interface displacements with respect to x are (see Appendix A):

$$(du/dx)^{(s)} = \frac{1-2\nu_s}{1-\nu_s}\frac{\sigma_{yy}(x)}{\bar{E}_s}$$

$$+ \frac{2}{\pi\bar{E}_s}\int_0^\infty \frac{\sigma_{xy}(\xi)}{\xi-x}d\xi + \frac{2}{x\pi\bar{E}_s}\int_0^\infty \left[\frac{\pi^2}{4-\pi^2}\right.$$

$$\left.+ \frac{\xi/x}{1+\xi/x} - k_1(\xi/x)\right]\sigma_{xy}(\xi)d\xi \qquad (13a)$$

$$+ \frac{2}{x\pi\bar{E}_s}\int_0^\infty \left[\frac{2\pi}{4-\pi^2} - k_2(\xi/x)\right.$$

$$\left.- k_3(\xi/x)\right]\sigma_{yy}(\xi)d\xi,$$

$$(dv/dx)^{(s)} = \frac{1-2\nu_s}{1-\nu_s}\frac{\sigma_{xy}(x)}{\bar{E}_s}$$

$$+ \frac{2}{\pi\bar{E}_s}\int_0^\infty \frac{\sigma_{yy}(\xi)}{\xi-x}d\xi + \frac{2}{x\pi\bar{E}_s}\int_0^\infty \left[\frac{\pi^2}{4-\pi^2}\right.$$

$$\left.+ \frac{\xi/x}{1+\xi/x} - k_1(\xi/x)\right]\sigma_{yy}(\xi)d\xi \qquad (13b)$$

$$+ \frac{2}{x\pi\bar{E}_s}\int_0^\infty \left[\frac{2\pi}{4-\pi^2} + k_2(\xi/x)\right.$$

$$\left.- k_3(\xi/x)\right]\sigma_{xy}(x)d\xi,$$

In the right hand sides of both equation (13a) and equation (13b), the first two terms correspond to the half plane solution and the last two integrals represent the effect of the edge of the substrate. The three kernel functions $k_i(\xi)$ ($i = 1, 3$) are all regular and finite functions. They are specified and plotted in Appendix A. In equation (13), the origin of the coordinate system is set at the corner of the substrate. One can show that the brackets in the second or third integrals in equation (13a) and equation (13b) all approach zero as $\xi/x\to\infty$. The contributions from the last two integrals in equation (13a) and equation (13b) approach zero at values of x remote from the corner. Since the effects of the substrate edge on interface deformation decays as $1/(\bar{E}_s x)$, one can anticipate that the energy release rate for the crack emerging from a corner edge (Fig. 2(b)) will slowly approach steady state if the substrate is not very stiff. This will be seen to be the case.

3. INTERFACE CRACKING FROM A FILM EDGE: INTERIOR VERSUS CORNER EDGES

The problems in Fig. 2(a) and (b) are considered first, employing equation (10) for the semi-infinite substrate and equation (13) for the quarter plane substrate. The integral equations are cast into non-dimensional form by normalizing stresses by σ_0, lengths by h, and displacements by $h\sigma_0/\bar{E}_f$, where $\bar{E} = E/(1-\nu^2)$. The combinations of elastic constants appearing in the non-dimensional integral equations can be fully expressed in terms of the two Dundurs parameters:

$$\alpha = \frac{\bar{E}_f - \bar{E}_s}{\bar{E}_f + \bar{E}_s}, \beta = \frac{1}{2}\frac{\mu_f(1-2\nu_s)-\mu_s(1-2\nu_f)}{\mu_f(1-\nu_s)+\mu_s(1-\nu_f)}$$

$$(14)$$

where $\mu = E/[2(1 + \nu)]$. Usually, β plays a secondary role in the class of problems under consideration. Because the discussion of mixed mode effects is simplified when $\beta = 0$ [12], numerical solution has been restricted to these cases. The mode I and II stress intensity factors, and K_I and K_{II}, can be computed directly as the amplitudes of the square-root singular terms representing the traction distributions. The energy release rate and measure of mode mix are given by

$$G = \frac{1}{2}\left(\frac{1}{\bar{E}_f} + \frac{1}{\bar{E}_s}\right)(K_I^2 + K_{II}^2), \qquad (15)$$

$$\tan\psi = \frac{K_{II}}{K_I} \,(\beta = 0)$$

Alternatively, G can be computed by directly calculating the energy in the system at two slightly different crack lengths and forming a numerical derivative. This method leads to somewhat higher accuracy than the first of equation (15), and it was used to generate the numerical results presented in the paper.

3.1. Energy release rate and mode mix

The energy release rate of a crack emerging from an *interior edge* (Fig. 2(a)) is within a few percent of the steady-state limit, G_{ss}, given by equation (1) for crack lengths, a, which are less than $h/2$, as can be seen in Fig. 6. There is essentially no dependence on the elastic mismatch parameter α when the crack is longer than $h/2$. The solid curves in Fig. 6 are the predictions of the present model. The solid dots (at $a/h = 0.1, 0.5, 1$ and 2) have been computed using a finite element model for the case of no elastic mismatch. These substantiate the present results. For a/h even smaller than 0.1, G necessarily must go to zero as a/h goes to zero, but no attempt has been made to resolve that dependence. The present model is not intended for predicting behavior of such short cracks, as will be discussed further below. The dependence
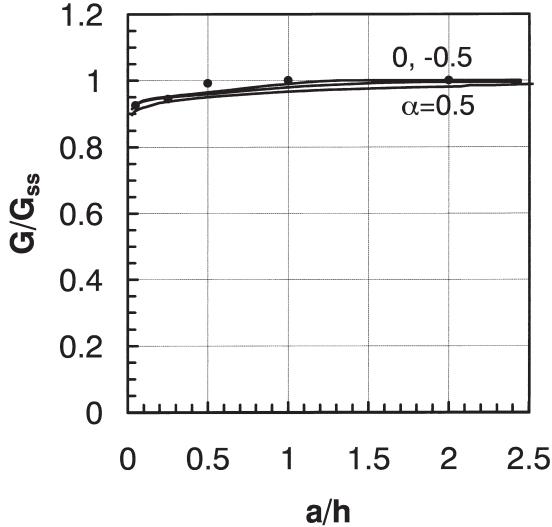
Fig. 6. Energy release rate as a function of crack length for a crack emerging at an interior edge ($\beta=0$). The solid dots were calculated using a finite element method for the case of $\alpha=0$.

of the mode mix for the interior edge has not been plotted because it also is essentially independent of crack length for $a/h > h/2$. The steady-state limit is $\psi_{ss} = \omega(\alpha)$, where $\omega(\alpha)$ is given in [12]. In the absence of elastic mismatch, $\omega(0) = 52.1°$, corresponding to nearly equal proportions of modes I and II. Look ahead to Fig. 8 to see the influence of α on ψ_{ss}.

The main inference to be drawn from the results in Fig. 6 is that there is a very small barrier to initiation of crack propagation for an interface crack emerging from an interior edge. An initial interface flaw whose length is only a small fraction of the film thickness will be almost as lethal as a much longer

crack. The situation for a crack emerging from a *corner edge* (Fig. 2(b)) is very different, as can be seen in Fig. 7. In this case, the energy release rate has a slow approach to the steady-state limit as the crack length increases. The solid curves are the predictions of the present model, and the solid points are the predictions from a finite element calculation. The energy release rate emerges from zero at $a/h = 0$ and attains 95% of G_{ss} only when a/h exceeds 10 or more. The elastic mismatch parameter, α, has a quantitative influence on G, such that an interface crack between a compliant film and stiff substrate ($\alpha = -0.5$) approaches steady-state at much shorter crack lengths, and vice versa for $\alpha = 0.5$. Remarkably, only when $a/h = 40$ does the crack attain 90% of G_{ss} for a film that is three times as stiff as the substrate ($\alpha = 0.5$). It is notable that the mode mix, ψ, in Fig. 8 is close to its steady-state value at relatively short crack lengths, typically $a/h = 1$ or shorter, depending on the elastic mismatch. The influence of elastic mismatch on the approach to the steady-state limit is well captured by plotting G/G_{ss} as a function of $\bar{E}_f h/(\bar{E}_s a)$. As seen in Fig. 9, the results plotted this way for the three elastic mismatches nearly collapse to a single curve for $G/G_{ss} > 0.6$ with an initial slope of -1.

Together, Fig. 6 and Fig. 7 highlight one of the main findings in this paper: interior edges of a thin film are inherently more susceptible to delamination than corner edges.

3.2. Interface stress distribution

Figure 10(a) and (b) show the tractions along the interface as computed by the present model for the configuration shown in Fig. 2(a), a semi-infinite film with an interior edge. Since a stiffer substrate imposes stronger constraint on the thin film, the stress near the crack is higher for $\alpha = -0.5$ than the other two
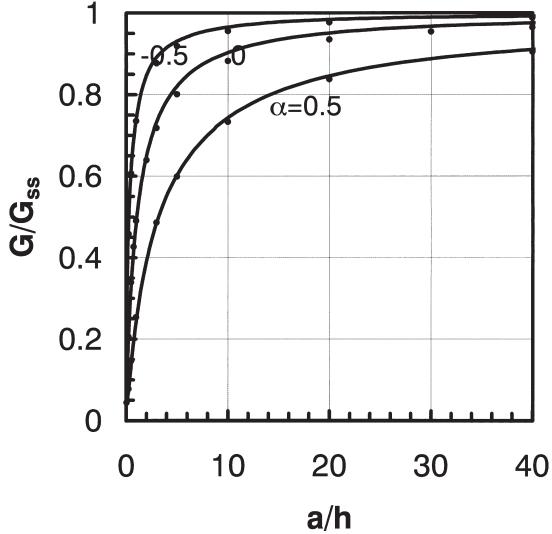
Fig. 7. Normalized energy release rate as a function of crack length for a crack emerging at a corner edge. The solid dots were calculated using a finite element representation.
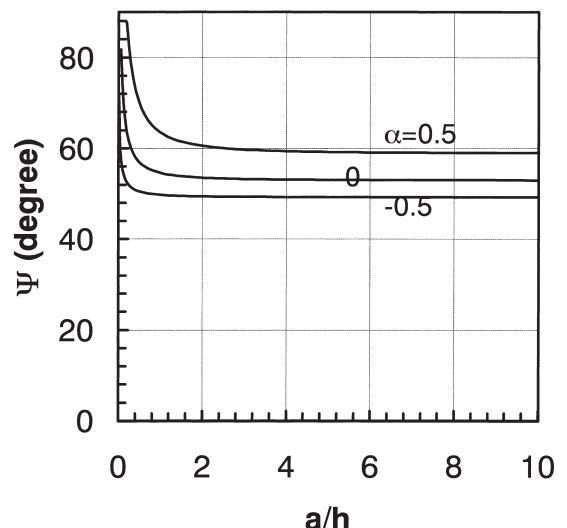
Fig. 8. Measure of mode mix as a function of crack length for a crack emerging at a corner edge.
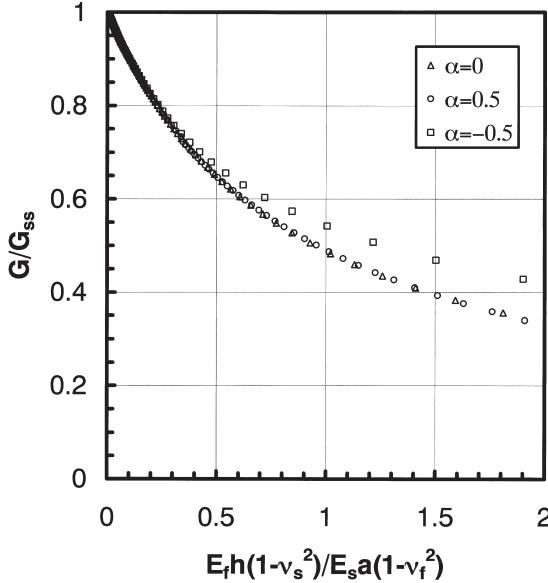
Fig. 9. Energy release rate plotted against the normalization $(1-v_s^2)E_t h/[(1-v_f^2)E_s a]$.

Fig. 10. Shear stress (a) and normal stress (b) acting on the interface ahead of the crack tip for the geometry in Fig. 2(a).

cases. The normal stress is tensile near the crack tip and turns compressive within a zone less than one film thickness.

The model gives the same stress distribution along the interface in Fig. 2(a) whether or not a crack is present. The solution is independent of the crack length, assuming the origin is taken at the crack tip. The models proposed by Freund and Hu [8] and Shield and Kim [9] have the same feature. When the crack length is greater than about $h/4$, the actual stress distribution along the interface is almost the same as the steady state solution because the effect of the free detached edge of the film has negligible effect except within $h/4$ from the attachment point. Moreover, the actual interface traction distribution for the case without an interface crack is almost the same as the case with crack except in a zone near the edge about $h/4$ in width. The following observations shed light on this and related features. The net force and moment exerted by the detached end of the film on the attached film to the right of $x = 0$ is zero. Therefore, an Airy stress function representing the effect of the detached film on the attached portion can be written as a series of biharmonic eigen-functions, which are of the form [13, 14]

$$\Phi_{\text{even}} = e^{-\gamma_n x/h}(\kappa_n \cos(\gamma_n y/h) + \gamma_n y/h \sin(\gamma_n y/h))$$

$$\Phi_{\text{odd}} = e^{-\gamma_n x/h}(\kappa_n \sin(\gamma_n y/h) + \gamma_n y/h \cos(\gamma_n y/h)).$$

$$(16)$$

The slowest decay mode has the real part of γ_n being 4.212, indicating the effects of the end load decay exponentially with a characteristic length about $h/4$ and can be ignored when the distance to film edge

is larger than that characteristic length. This is the underlying analytical reason that the energy release rate in Fig. 6 approaches steady-state for cracks of length under one film thickness. We emphasize again that no effort has been made to resolve behavior for even shorter cracks, which can be important in certain applications. The recent work by Liu, Suo and Ma [15] provides details of stress distributions in the immediate vicinity of a film edge when there is no crack.

Figure 11(a) and (b) compare the stress distributions from the three models for the case of no elastic mismatch, along with a finite element solution for a crack with $a/h = 5$. The stresses are multiplied by $\sqrt{2\pi x/h}$ to remove the singularity at the crack tip. The horizontal lines in Fig. 11(a) and (b) represent the

(a)

(b)
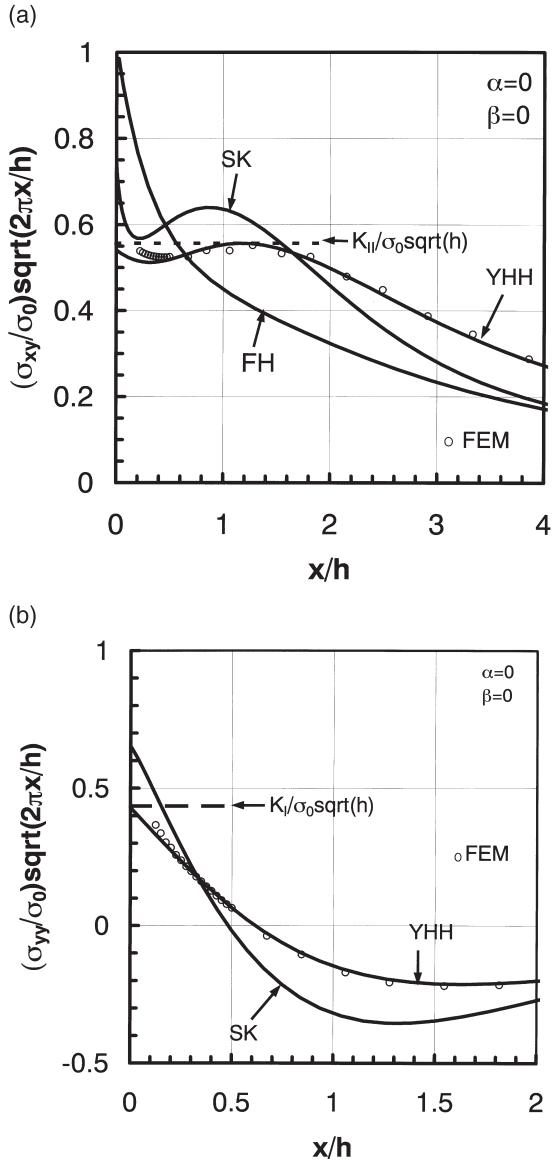
Fig. 11. Normalized shear stress (a) and normal stress (b) acting on the interface for the geometry of Fig. 2(a) according to three models (Freund and Hu (FH), Shield and Kim (SK) and the present model (YHH)) and a finite element calculation (open circles). The exact limit as the tip is approached is also shown.

exact results for $K_{II}/\sigma_0\sqrt{h}$ and $K_I/\sigma_0\sqrt{h}$, respectively, for the steady state crack [12]. The differences among the solutions are apparent. The present model (YHH) gives accurate results for both the stress intensity factors and the full traction distributions. The model of Shield and Kim (SK) has a similar trend, but with significant error in prediction of the stress intensity factors. It is worth noting that the normal stress diverges quickly from the asymptotic solution as x increases and turns compressive at about $0.6h$. This suggests that the zone of dominance of the intensity field tied to K_I will be a small fraction of the film thickness. The ratio of the normal to the shear traction also changes rapidly when x increases, indicating that

the mode mix calculated from the limit value at the crack tip only has a very limited domain of validity.

The traction distributions along the interface as obtained from the present model for a perfectly bonded thin film without a crack whose edge is aligned with the corner of the substrate (Fig. 2(b)) are plotted as solid curves in Fig. 12 (a) and (b). The discrete points in Fig. 12(b) for the normal stress are the results of a finite element calculation. These further reinforce the accuracy of the present model.

4. STRESSES FOR FINITE WIDTH FILMS

Now the focus will be on the interaction between the two edges of a finite width film as a prelude to the converging debond study. The interface traction for thin film with finite width, $2L$, fully bonded to the

(a)

(b)
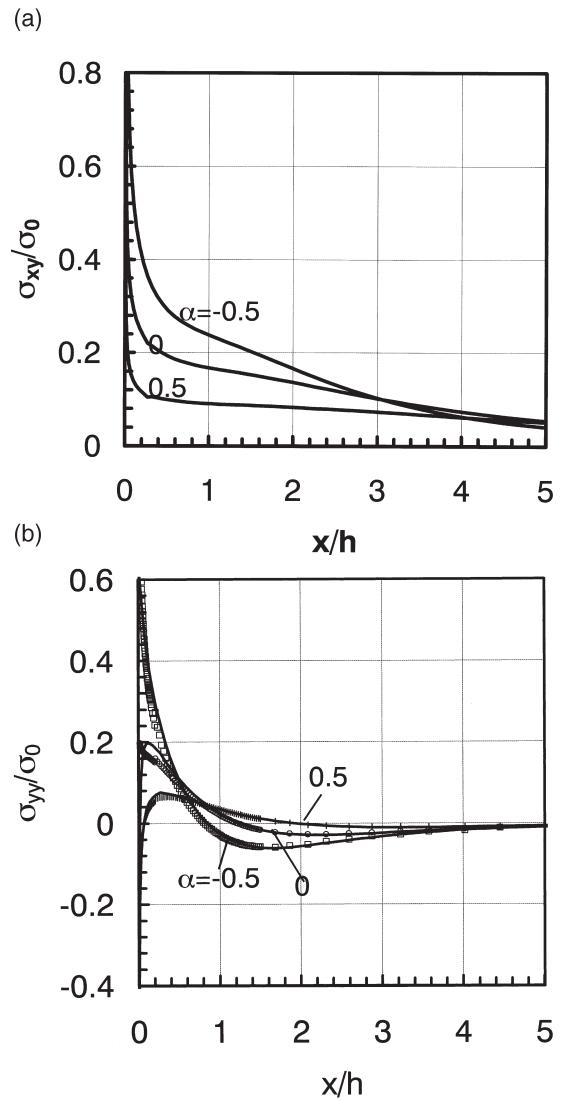
Fig. 12. Shear stress (a) and normal stress (b) acting on the interface for a film whose edge is aligned with a corner of the substrate (Fig. 2(b), but without a crack). The discrete points in (b) are the results of a finite element calculation.

top of a half space (Fig. 3(a)) can also be computed. Of particular interest is the distribution of the residual stress averaged through the thickness direction,

$$\sigma_{avg}(x) = (1/h)\int_0^h \sigma_{xx}(x,y)dy,$$ which can be calculated

from the shear stress distribution along the interface. The strong interaction between the two ends is seen in Fig. 13, where the average residual stress distribution is plotted for $\alpha = 0.5$ and -0.5. The average stress has a maximum at the mid point, $x = 0$, but it only approaches σ_0 when the width of the film is greater than 100 h or more, depending on the elastic mismatch. Similar results were obtained in [9]. The maximum residual film stress can be significantly below σ_0 when the width of the film is in the range from 5 to 10 h.

The long-range interaction between the two edges can be understood as follows. The two edges communicate with each other not only through the film itself, but also through the substrate. In fact, the stress relaxation in the film is mainly due to the deformation of the substrate when $L/h\gg1$. If $L/h\gg1$ and the stress well away from the edge is of interest, the concentrated shear traction near the two edges can be treated as two equal and opposite point forces acting on the substrate. By matching the horizontal strain, du/dx, of the thin film and the substrate at the middle of the bonded interface, one obtains the following estimate of the average stress at the middle cross section, σ_{avg}:

$$1-\sigma_{avg}/\sigma_0 = \frac{4h\bar{E}_f}{\pi L\bar{E}_s}, \qquad (17)$$

Only the lowest order of influence of h/L has been retained in equation (17). The accuracy of equation (17) is apparent from Fig. 14, where the solid lines are plotted using equation (17) and the solid points represent values of σ_{avg} computed using the present model. The long range interaction between the edges is a consequence of the deformation of the substrate, which in turn is related to the $1/x$ long range dependence of the strain in the substrate when acted upon by a concentrated force.
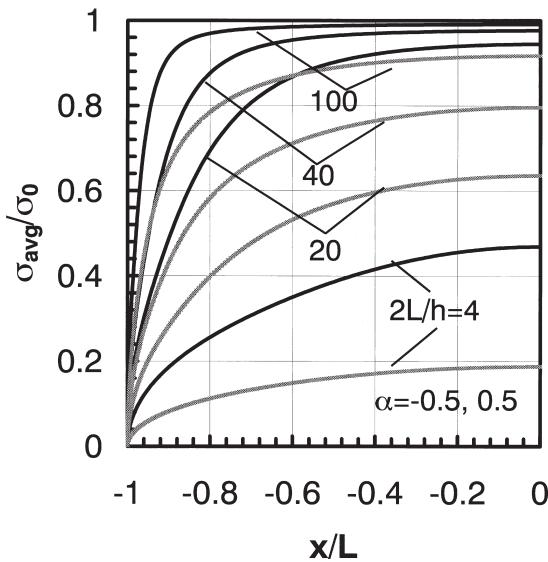
5. CONVERGING DEBONDS

The results for the finite width films in the previous section have relevance to the problem of an interface crack approaching an interior edge (Fig. 2(c)). The interaction of the crack tip and the edge of the film is similar to that of the two edges. The crack begins to relax the residual stress and strain energy in the attached segment of the film when the attachment width, b, is many times the film thickness. As a consequence, the energy release rate begins to drop below the steady state value when b/h is quite large, as seen in the curves of Fig. 15(a). A stiff film on a compliant substrate (e.g., $\alpha = 0.5$) displays a 20% drop in the energy release rate when b/h is 25. Even in the absence of elastic mismatch a similar reduction occurs when b/h is 10. This gradual fall off in the energy release rate was exploited in [3] to measure the interface toughness of films which had been stressed to the point where G_{ss} exceeded the interface toughness. They used measured values of b/h at arrest to infer the critical energy release rate. He *et al.* [4] carried out finite element calculations for convergent debonding of thin films, detailing behavior similar to that seen in Fig. 15(a). The associated measure of mode mix is plotted in Fig. 15(b). Unlike G, ψ

Fig. 13. Interaction effect between film edges. Average of the residual in-plane stress in films extending from $x=-L$ to $x=L$ for two elastic mismatches. For each pair of curves, the lower curve is for $\alpha=0.5$.
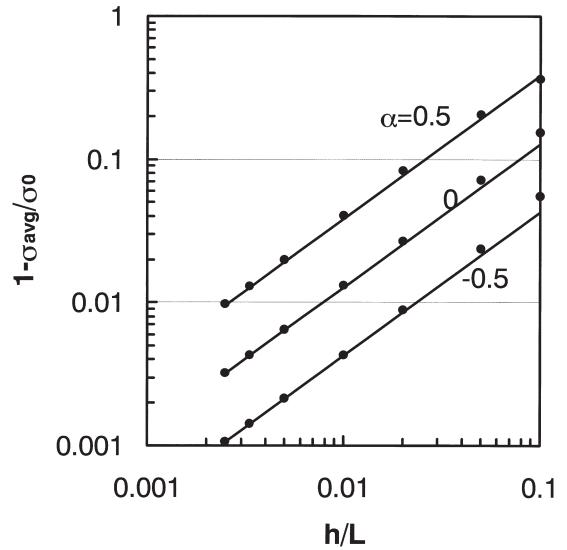
Fig. 14. Comparison in the reduction of the average residual stress at the center of a film of width $2L$ as predicted by the simple formula Eq. (17) and the predictions of the present model.

(a)

(a)

(b)
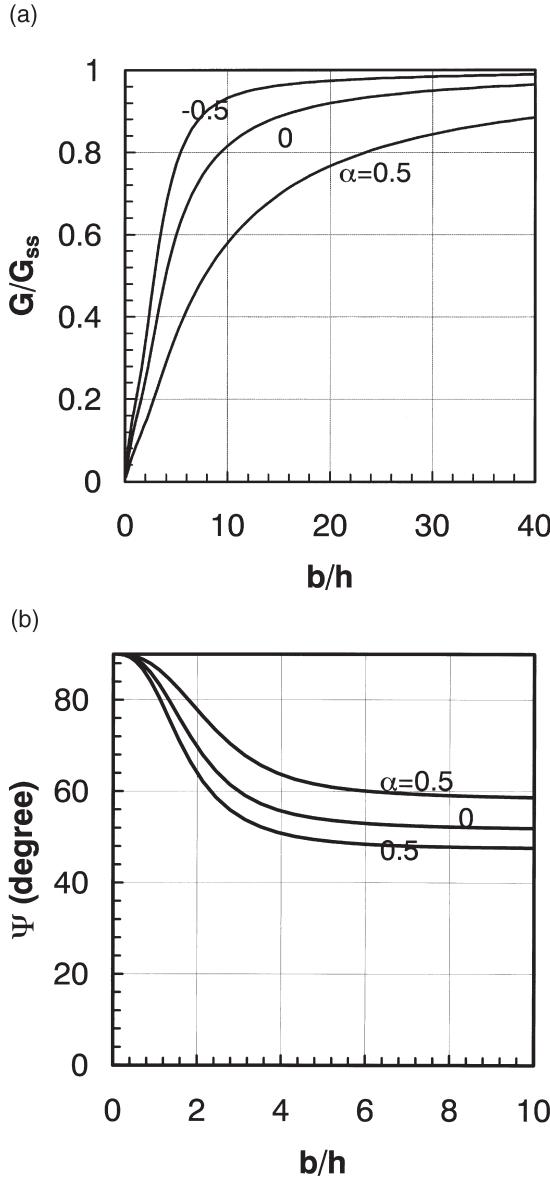
Fig. 15. Energy release rate (a) and mode mixity (b) for an interface crack converging on an interior edge (Fig. 2(c)).

(b)

Fig. 16. Energy release rate (a) and mode mixity (b) for an interface crack converging on a corner edge (Fig. 2(d)).

remains close to the steady state until the remaining ligament is relatively small. The significance of this for testing based on convergent debonding is that the toughness measured will be associated with the steady state mode mix, unless b/h at arrest is less than about 4.

Results for an interface crack converging on a corner edge (Fig. 2(d)) are given in Fig. 16(a) and (b). The behavior is qualitatively similar. Now, however, the crack tip "feels" the corner edge at even greater distances than for the interior edge. A 20% reduction in the energy release rate already occurs when $b/h = 40$ for $\alpha = 0.5$. For reasons discussed earlier, the present model loses accuracy when b/h is on the order of unity.

Further evidence to support the very small influ-

ence that the detached segment of the film has on the stress distribution (cf. Section 3.2) is provided by the following observation. The energy release rate of the interface cracks for the two configurations in Fig. 17(a) and (b) are indistinguishable from one another when the remaining ligaments satisfy $b/h > 1/2$ [4]. The present model predicts that these two cases have precisely the same energy release rates. Similarly, one could also expect that the interface tractions for all three cases in Fig. 17 are essentially identical except for the zones on the order of $1/4\,h$ very close to the film edges. As already mentioned, the present model is not able to resolve such distinctions; it predicts that the stress distribution for all three cases in Fig. 17 is the same.
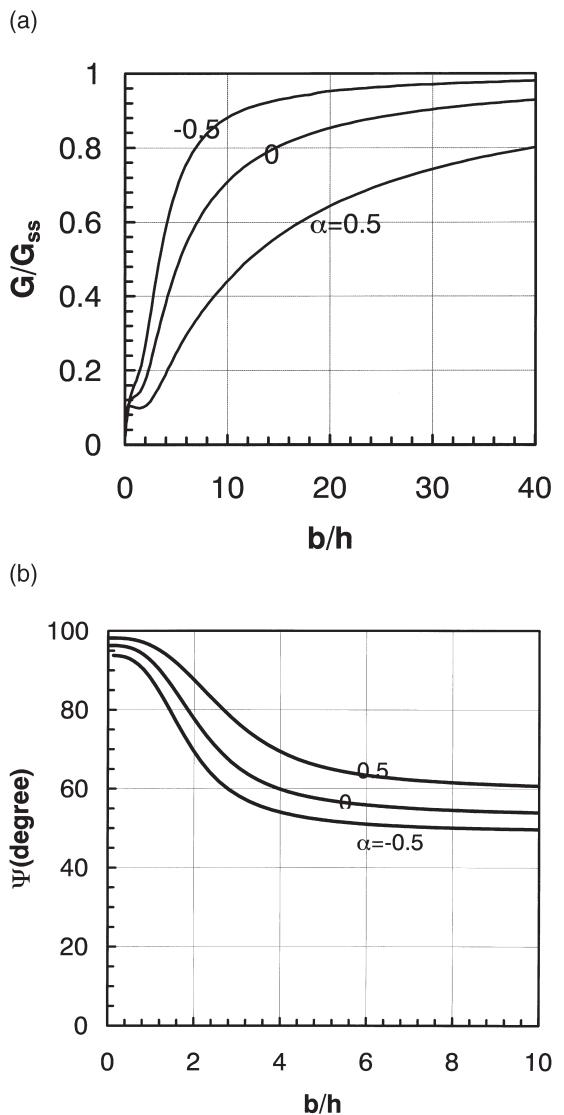
(a)

(a)

(b)

(c)
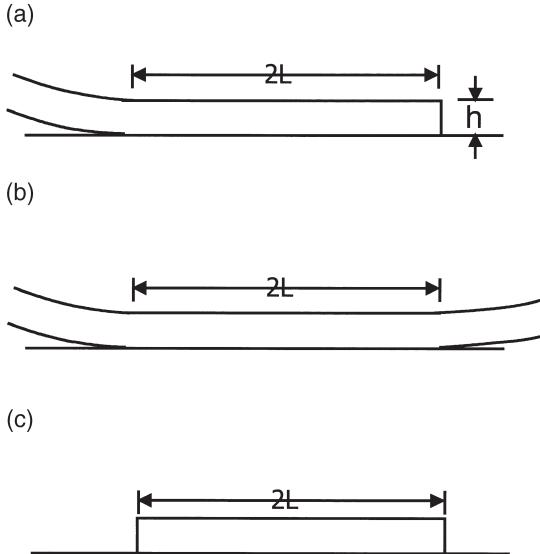
Fig. 17. Three film geometries that have nearly identical stress distributions everywhere except within a distance of about $h/4$ from the edges.

(b)

6. CONCLUDING REMARKS

Edges profoundly influence the stress distribution and the energy release rates of interface cracks of thin films. Moreover, there are important differences between the behaviors of cracks emerging from interior edges and corner edges. Interface cracks emerging from an interior edge approach the full steady state energy release rate equation (1) remarkably quickly, at distances of a fraction of a film thickness from the edge. By contrast, a crack emerging from an edge at the corner of a substrate remains well below the steady state energy release rate until the crack length is many times the film thickness. Only if the film is on a very stiff substrate will the approach to steady state cracking occur at relatively short crack lengths. In effect, corner edges provide an intrinsic protection against the nucleation of interface delaminations. Interior edges do not.

Interface cracks converging on an edge begin to "feel" the edge at distances that are many times the film thickness, whether the edge is at a corner or in the interior of the substrate. Delamination cracks approaching an edge will arrest at a well defined stand off distance where the energy release rate drops to the level of the interface toughness. This phenomenon is manifest in various observations of thin film delamination. An example is the partial delamination of residually stressed film strips which was observed in some of the experiments conducted by Zhuk *et al.* [3] and sketched in Fig. 18. The width of the strip of film, $2L$, is large compared to the film thickness, say $2L/h \cong 50$. In instances when full delamination occurred, the interface crack starts at one end, debonds the full width of the strip, and arrests as it converges on the other end. Many of the strips behaved in this manner. However, for some strips, the
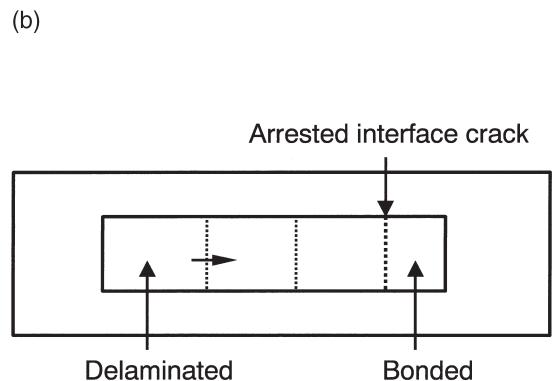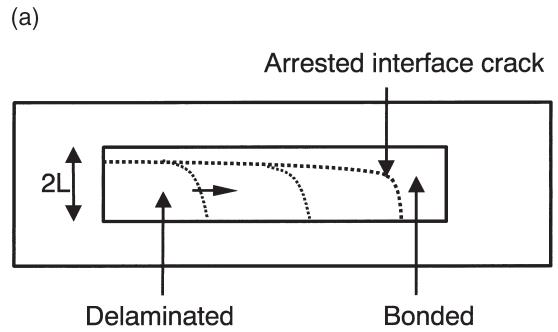
Fig. 18. Two observed modes of delamination of film strips: partial-width debonding and full-width debonding. The average energy release rate for partial-width debonding is larger than for full-width debonding. (a) Partially delamianted; (b) fully delaminated.

interface crack emerges from the end of the film and spreads along the film without debonding the full width of the film, as depicted in Fig. 18. The propagating partial-width crack arrested as it converged with the far end of the film. Based on the results presented in Section 3 and Section 5, one can readily see that the average energy release rate of the interface crack in the partially delaminated strip must be greater than that for the fully delaminated case, at a given reference stress, σ_0. In other words, partial delamination is energetically favored above full delamination in the sense that it could occur at lower σ_0.

The modeling approach presented in Section 2 is somewhat more complicated than earlier models, but, nevertheless, leads to the same general class of integral equations obtained in the earlier models and these can be solved with the same numerical methods. One obvious virtue of the new approach is that it preserves the precise form of the singularity field of the interface crack. Equally important, it has been demonstrated to be highly accurate, except for very short cracks near the edges of the film.

Finally, the residual stress has been assumed to be tensile in this paper. When the residual stress is compressive, the two crack surfaces will be in contact. In this case, the relations between the derivatives of the

displacements and tractions on the interface expressed in equation (2), equation (3), equation (7), equation (9) and equation (10) are still valid. The traction free condition along the crack surface should be replaced by an appropriate contact condition thereby establishing the modified integral equations. This will be pursued elsewhere.

APPENDIX A

The stresses in a wedge (Fig. 19) with a normal point force F_n exerting on one of the wedge surfaces ($\theta = \alpha$) are obtained using a Mellin transformation as proposed by Tranter [16].

$$r(\sigma_\theta + \sigma_r) = F_\text{n}\frac{\sin 2\alpha \sin(\alpha + \theta) + 2\alpha \sin(\theta-\alpha)}{\sin^2 2\alpha-4\alpha^2}$$

$$+ \frac{F_\text{n}}{\pi}\int_0^\infty\left\{\left[-\frac{T(\xi)}{G(\xi)} + \frac{Q(\xi)}{H(\xi)}\right]\cos\left(\xi \ln\frac{d}{r}\right) + \left[\frac{S(\xi)}{G(\xi)}\right.\right.$$
$$\left.\left.-\frac{P(\xi)}{H(\xi)}\right]\sin\left(\xi \ln\frac{d}{r}\right)\right\}d\xi$$

$$r(\sigma_\theta-\sigma_r) = -F_\text{n}\frac{\sin 2\alpha \sin(\alpha + \theta) + 2\alpha \sin(\theta-\alpha)}{\sin^2 2\alpha-4\alpha^2}$$

y axis, Fn, Ft, x axis, α, -α, (r,θ)
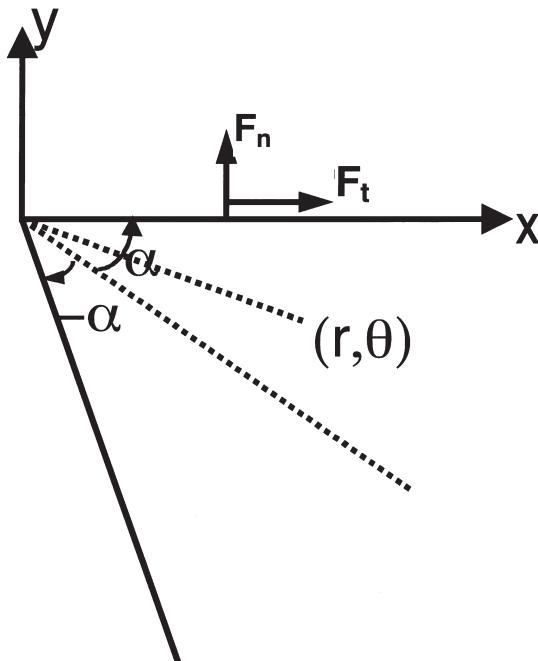
Fig. 19. Conventions for the solution for the substrate with a corner.

$$+ \frac{F_\text{n}}{\pi}\int_0^\infty\left[-\frac{S(\xi)}{G(\xi)} + \frac{P(\xi)}{H(\xi)}\right]\left[\xi \cos\left(\xi \ln\frac{d}{r}\right)\right.$$
$$\left.+ \sin\left(\xi \ln\frac{d}{r}\right)\right]d\xi$$

$$r\sigma_{r\theta} = \frac{F_\text{n}}{2\pi}\int_0^\infty\left[\frac{U(\xi)}{G(\xi)}-\frac{R(\xi)}{H(\xi)}\right]\left[\cos\left(\xi \ln\frac{d}{r}\right)\right.\quad\text{(A1)}$$
$$\left.-\xi \sin\left(\xi \ln\frac{d}{r}\right)\right]d\xi$$

and the stresses in a wedge with a tangential point force F_t exerting on one of the wedge surfaces

$$r(\sigma_\theta + \sigma_r)$$
$$= F_\text{t}\frac{-\sin 2\alpha \cos(\alpha + \theta) + 2\alpha \cos(\theta-\alpha)}{\sin^2 2\alpha-4\alpha^2} + \frac{F_\text{t}}{\pi}\int_0^\infty\left\{\left[\right.\right.$$
$$\left.-\frac{R(\xi)}{G(\xi)} + \frac{U(\xi)}{H(\xi)}\right]\cos\left(\xi \ln\frac{d}{r}\right) + \left[\frac{O(\xi)}{G(\xi)}\right.$$
$$\left.\left.+ \frac{V(\xi)}{H(\xi)}\right]\sin\left(\xi \ln\frac{d}{r}\right)\right\}d\xi$$

$$r(\sigma_\theta-\sigma_r) = F_\text{t}\frac{\sin 2\alpha \cos(\alpha + \theta)-2\alpha \cos(\theta-\alpha)}{\sin^2 2\alpha-4\alpha^2}$$
$$+ \frac{F_\text{t}}{\pi}\int_0^\infty\left\{\left[\frac{O(\xi)}{G(\xi)}-\frac{V(\xi)}{H(\xi)}\right] + \xi\left[-\frac{R(\xi)}{G(\xi)}\right.\right.$$
$$\left.\left.+ \frac{U(\xi)}{H(\xi)}\right]\right\}\sin\left(\xi \ln\frac{d}{r}\right)d\xi$$

$$r\sigma_{r\theta} = \frac{F_\text{t}}{2\pi}\int_0^\infty\left\{\left[-\frac{Q(\xi)}{G(\xi)} + \frac{T(\xi)}{H(\xi)}\right] + \xi\left[\frac{P(\xi)}{G(\xi)}\right.\right.\quad\text{(A2)}$$
$$\left.\left.-\frac{S(\xi)}{H(\xi)}\right]\right\}\cos\left(\xi \ln\frac{d}{r}\right)d\xi$$

where

$$G(\xi) = \xi \sin 2\alpha-\sinh(2\xi\alpha)$$

$$H(\xi) = \xi \sin 2\alpha + \sinh(2\xi\alpha)$$

$$P(\xi) = \sin(\alpha-\theta)\cosh((\alpha + \theta)\xi) + \sin(\alpha + \theta)\cosh((\alpha-\theta)\xi)$$

$$Q(\xi) = \cos(\alpha-\theta)\sinh((\alpha + \theta)\xi) + \cos(\alpha$$

$$+ \theta)\sinh((\alpha - \theta)\xi)$$

$$R(\xi) = \sin(\alpha - \theta)\sinh((\alpha + \theta)\xi) - \sin(\alpha + \theta)\sinh((\alpha - \theta)\xi)$$

$$O(\xi) = \cos(\alpha - \theta)\cosh((\alpha + \theta)\xi) - \cos(\alpha + \theta)\cosh((\alpha - \theta)\xi)$$

$$S(\xi) = \sin(\alpha - \theta)\cosh((\alpha + \theta)\xi) - \sin(\alpha + \theta)\cosh((\alpha - \theta)\xi)$$

$$T(\xi) = \cos(\alpha - \theta)\sinh((\alpha + \theta)\xi) - \cos(\alpha + \theta)\sinh((\alpha - \theta)\xi)$$

$$U(\xi) = \sin(\alpha - \theta)\sinh((\alpha + \theta)\xi) + \sin(\alpha + \theta)\sinh((\alpha - \theta)\xi)$$

$$V(\xi) = \cos(\alpha - \theta)\cosh((\alpha + \theta)\xi) \quad \text{(A3)}$$
$$+ \cos(\alpha + \theta)\cosh((\alpha - \theta)\xi).$$

On the surface of $\theta = \alpha$, the derivatives of the displacement with respect to r are calculated for both cases. When the surface is subjected to distributed normal and shear tractions, the derivatives of displacement with respect to r can be obtained by linear superposition. After lengthy algebraic manipulation, one has

$$\frac{\mathrm{d}u}{\mathrm{d}r} = \frac{1 - 2v}{1 - v}\frac{\sigma_{yy}(r)}{\bar{E}} + \frac{1}{r}\int_0^\infty \left[\frac{2\alpha - \sin 2\alpha \cos 2\alpha}{\sin^2 2\alpha - 4\alpha^2}\right.$$
$$+ \frac{1}{2\alpha}\frac{\xi^{\pi/2\alpha} + r^{\pi/2\alpha}}{\xi^{\pi/2\alpha} - r^{\pi/2\alpha}} - \frac{2 \sin^2 2\alpha}{\pi}k_1(\xi/r)\left]\frac{\sigma_{xy}(\xi)}{\bar{E}}\mathrm{d}\xi\right.$$
$$+ \frac{1}{r}\int_0^\infty \left[\frac{\sin^2 2\alpha}{\sin^2 2\alpha - 4\alpha^2} - \frac{\sin^2 2\alpha + \sin 2\alpha}{\pi}k_2(\xi/r)\right.$$
$$- \frac{2 \sin 2\alpha}{\pi}k_3(\xi/r)\left]\frac{\sigma_{yy}(\xi)}{\bar{E}}\mathrm{d}\xi\right.$$

$$\frac{\mathrm{d}v}{\mathrm{d}r} = -\frac{1 - 2v}{1 - v}\frac{\sigma_{xy}(r)}{\bar{E}}$$
$$+ \frac{1}{r}\int_0^\infty \left[\frac{2\alpha + \sin 2\alpha \cos 2\alpha}{\sin^2 2\alpha - 4\alpha^2}\right.$$
$$+ \frac{1}{2\alpha}\frac{\xi^{\pi/2\alpha} + r^{\pi/2\alpha}}{\xi^{\pi/2\alpha} - r^{\pi/2\alpha}}$$
$$- \frac{2 \sin^2 2\alpha}{\pi}k_1(\xi/r)\left]\frac{\sigma_{yy}(\xi)}{\bar{E}}\mathrm{d}\xi \quad \text{(A4)}\right.$$
$$+ \frac{1}{r}\int_0^\infty \left[\frac{\sin^2 2\alpha}{\sin^2 2\alpha - 4\alpha^2}\right.$$

$$+ \frac{3 \sin^2 2\alpha - \sin 2\alpha}{\pi}k_2(\xi/r)$$
$$- \frac{2 \sin 2\alpha}{\pi}k_3(\xi/r)\left]\frac{\sigma_{xy}(\xi)}{\bar{E}}\mathrm{d}\xi\right.$$

where

$$k_1(\xi/x)$$
$$= \int_0^\infty \frac{\eta^2}{\eta^2 \sin^2 2\alpha - \sinh^2 2\alpha\eta}\frac{\cosh 2\alpha\eta}{\sinh 2\alpha\eta}\sin(\eta \ln \xi/x)\mathrm{d}\eta$$

$$k_2(\xi/x) = \int_0^\infty \frac{\eta^2}{\eta^2 \sin^2 2\alpha - \sinh^2 2\alpha\eta}\cos(\eta \ln \xi/x)\mathrm{d}\eta$$

$$k_3(\xi/x) = \int_0^\infty \frac{\eta^2}{\eta^2 \sin^2 2\alpha - \sinh^2 2\alpha\eta}$$
$$\sin(\eta \ln \xi/x)\mathrm{d}\eta. \quad \text{(A5)}$$

The first term in the right hand side of each equation in equation (A4) represents the effect of the local stress on the deformation. It is obtained after calculating the residue of the corresponding integral. The integrals in equation (A4) are defined as the Cauchy principal value where there are Cauchy-type kernels. The functions k_1, k_2, and k_3 are all regular and well defined.

As $\xi/x \to \infty$, $k_1 \to \{\pi/[4\alpha(\sin^2 2\alpha - 4\alpha^2)]\}$, $k_2 \to 0$ and $k_3 \to \{\pi/[2(\sin^2 2\alpha - 4\alpha^2)]\}$. For a quarter plane, $\alpha = \pi/4$, the corresponding k_1, k_2 and k_3 are plotted in Fig. 20.
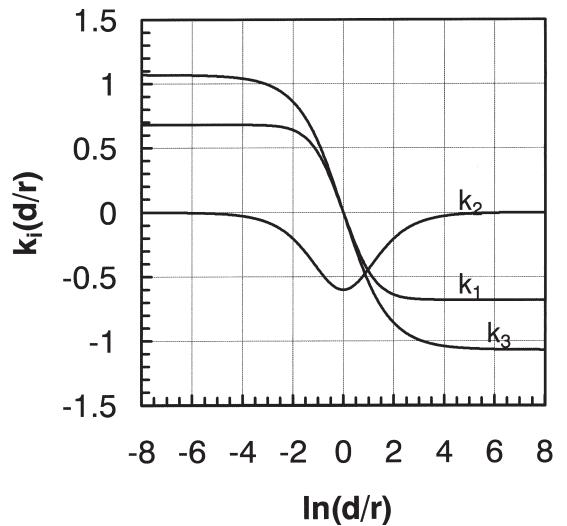
Fig. 20. Functions characterizing the behavior for a substrate with a corner.

The solutions for the point forces on another surface $\theta = -\alpha$ are similar to equation (A1) and equation (A2) with only some change on the signs of some terms.

REFERENCES

1. Cannon, R. M., Fisher, R. M. and Evans, A. G., *Mater. Res. Soc. Symp. Proc.*, 1986, **54**, 799.
2. Thouless, M. D., Evans, A. G., Ashby, M. F. and Hutchinson, J. W., *Acta Metall.*, 1987, **35**, 1333.
3. Zhuk, A., Evans, A. G., Whitesides, G. and Hutchsinson, J. W., *J. Mater. Res.*, 1998, **13**, 3555.
4. He, M. Y., Evans, A. G. and Hutchinson, J. W., *Acta Mater.*, 1997, **45**, 3481.
5. Ramirez, J. C., McNally, P. J., Cooper, L. S., Rosenberg, J. J., Freund, L. B. and Jackson, T. N., *IEEE Transactions on Electron Devices*. 1988, **35**, 1232–1240.
6. Koiter, W. J., *Quart. J. Mech. Appl. Math.*, 1955, **8**, 164.
7. Erdogan, F. and Gupta, G. D. *J. Appl. Mech.*, 1971, **38**, 937.
8. Freund, L.B. and Hu, Y., Brown University report. 1988.
9. Shield, T. W. and Kim, K. S., *Int. J. Solids Structure*. 1992, **29**, 1085.
10. Timoshenko, S. and Goodier, J. N., *Theory of Elasticity*. McGraw-Hill, Inc, 1951.
11. Erdogan, F., Gupta, G. D. and Cook, T. S., in *Methods of Analysis and Solutions of Crack Problems*. ed. G. C. Shih, Noordhoff, Leyden, 1973, pp. 368–425.
12. Hutchinson, J. W. and Suo, Z., *Advances in Applied Mechanics*. 1992, **29**, 63.
13. Fadle, J., *Ingenieur-archiv.*, 1941, **11**, 125.
14. Horvay, G. and Schenectady, N. Y., *J. Appl. Mech., Trans. ASME*. 1953, **57**, 87.
15. Liu, X. H., Suo, Z. and Ma, Q. *Acta Mater.*, 1999, **47**, 67.
16. Tranter, C. J., *Q. J. Mech. Appl. Math.*, 1948, **1**, 125.